Journal of Materials Chemistry C

ROYAL SOCIETY OF CHEMISTRY

PAPER

View Article Online
View Journal

Cite this: DOI: 10.1039/d6tc00403b

Light-induced deformation of side-chain azo-polyacrylate: insights from atomistic modeling

Dmitry A. Ryndyk,[ab] Olga Guskova [a] and Marina Saphiannikova *[ab]

Received 6th February 2026,
Accepted 17th March 2026

DOI: 10.1039/d6tc00403b

rsc.li/materials-c

Fully atomistic molecular dynamics simulations are used to investigate light-induced deformation in amorphous side-chain azo-polyacrylates with flexible spacers. Illumination is modeled *via* an effective orientation potential acting on azobenzene chromophores, allowing nanosecond time scales to be accessed without explicit photoisomerization. Polarized light induces rapid reorientation of azobenzene units perpendicular to the polarization direction, followed by a much slower response of the polymer backbone. Above the glass transition temperature, this separation of time scales results in an initial contraction and subsequent uniaxial elongation of the sample along the light polarization, driven by backbone alignment rather than backbone stretching. Below the glass transition, chromophore reorientation leads only to contraction, while backbone conformations remain frozen. The chain length is found to have little influence on the observed behavior for the non-entangled systems studied. Analysis of spacer conformations and complementary quantum-chemical calculations show that the flexible alkyloxy–ester spacer accommodates light-induced torque primarily through torsional rearrangements, weakening and delaying torque transfer to the backbone.

Introduction

Superficial restructuring of photosensitive polymers has matured in recent years from the inscription of regular sinusoidal structures by the interference pattern of laser beam[1–6] to the fabrication of intricate patterns by means of structured light.[7,8] Nowadays, the laser beam structure can be easily reshaped in a lab to produce any desired pattern using such tools as geometric phase elements (q-plates) or spatial light modulators.[9,10] These tools enable 2D control of the intensity, polarization and phase of the propagating beam in the transverse plane, while light-matter interactions can introduce additional spatial dependence along the propagation direction. For example, photosensitive azobenzene-containing polymers (azo-polymers) not only absorb the light but can also rotate the azimuth of polarization ellipse clockwise or anti-clockwise depending on the helicity of the light and the penetration depth.[11,12]

A unique property of side-chain azo-polymers is their ability to convert structured light irradiation into a well-defined stress field[13,14] as a result of the light-induced reorientation of azobenzene chromophores (azo-chromophores). The stress magnitude in each material point is proportional to the local light intensity, while the major and minor axes of polarization ellipse define the principal axes of stress tensor.[12] Linearly polarized light causes a uniaxial stretching/contraction of azo-polymers,[15–19] while elliptically polarized light evokes biaxial deformation.[12,20] Implementing the light field into the finite element software ANSYS, an excellent agreement with experimentally observed superficial restructuring of azo-polymer films[12,21] and reshaping of azo-polymer microobjects[14,19,22] has been achieved.

The long-term stability of the reshaped surfaces and objects is ensured by the use of amorphous azo-polymers whose glass transition temperature is sufficiently high and not affected by the light irradiation.[23] In such polymers the photosensitive azo-units are attached to the main chain *via* a short spacer. Computer simulations have verified that the orientation of azo-chromophores perpendicular to the polarization direction is transferred to the reorientation of polymer backbones along the same direction.[24,25] The models of amorphous azo-oligomers in the simulations were coarse-grained (azo-unit being represented either as Gay-Berne model (GB) or spherocylinder particle) and rather stiff. Not only torsional barriers were increased both in backbones and side-chains, but also a single spherical bead represented the spacer. The use of stiff models was motivated by the experiments of Bublitz *et al.*,[15] who studied light-induced elongation of azo-polyester droplets on the water surface. The monomeric unit of this stiff azo-polyester is shown in Fig. 1a. In the simulations,[24] the reorientation of the azo-oligomers was accompanied by a significant extension of the volume element along the polarization direction, reproducing the experimentally observed effect.[15] Due to a strong (fast rigid) coupling of side- and main chains, the latter were oriented under light irradiation on the same time scale as the azo-chromophores.

[a] *Division Theory of Polymers, Leibniz Institute of Polymer Research Dresden, 01069 Dresden, Germany*
[b] *Technische Universität Dresden, 01062 Dresden, Germany. E-mail: grenzer@ipfdd.de*

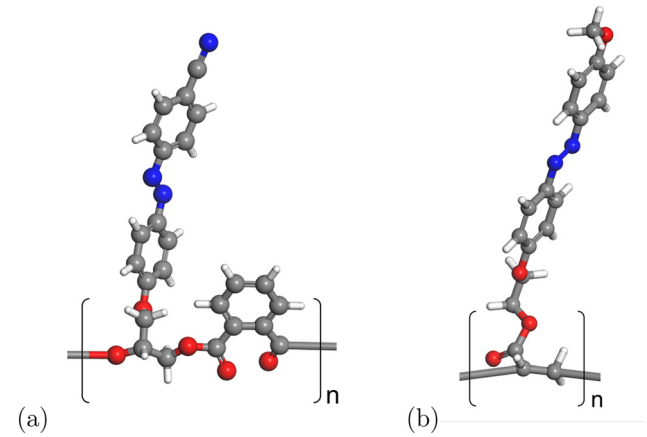

Fig. 1 (a) The monomeric unit of azo-polyester with a stiff backbone and an oxymethyl group as a short spacer to the azobenzene. (b) The monomeric unit of azo-polyacrylate with a flexible backbone and a longer spacer to azobenzene, consisting of ester- and ethyloxy groups.

Atomistic molecular dynamics (MD) simulations that explicitly include photoisomerization of azo-units have also been employed to study superficial restructuring of thin glassy azo-polymer films.[26,27] These simulations provide a microscopic description of how repeated *trans–cis–trans* cycles of the chromophores can trigger molecular migration and surface reshaping. However, due to the direct deposition of photon energy into the local degrees of freedom, such simulations are accompanied by pronounced transient heating in the irradiated regions, with temperatures reported up to 1800 K.[26] While these temperatures exceed the stability range of organic materials and therefore cannot be directly compared with experiment, they enable the mass transport process to be observed on the nanosecond timescales accessible to molecular dynamics of a side-chain azo-polymer. In parallel, theoretical approaches based on the reorientation of azo-chromophores,[13,28] describe the light-induced mass transport without invoking elevated temperatures. These models attribute the effect to anisotropic stresses arising from orientational ordering of polymer backbones and thus reproduce directional photodeformations and surface relief grating formation under near-ambient conditions.

Various azo-polymers have been utilized in the laboratories for superficial restructuring of thin films or for reshaping of micropillar arrays. Often polymers with flexible backbones and a spacer containing longer alkyl or alkyloxy groups have been used. For example, the spiral patterns in the experiment with helical beams were produced on the amorphous films of acrylic polymer with the methoxyazobenzene side-chain,[29] see Fig. 1b. The same polymer has been recently used to demonstrate the inscription capabilities of computer-generated holography.[30,31] For such a flexible polymer the coupling between the orientation of azo-containing side-chains and the backbones should be much weaker in comparison to the stiff azo-polyester discussed above. Nevertheless, the superficial restructuring is shown to be rather effective. This indicates that this polymer also effectively converts the structured light irradiation into the stress field which causes directional photodeformations.

To clarify the nature of the azo-backbone coupling, we perform in this study fully atomistic MD simulations of dense azo-polyacrylate samples in a wide range around their glass transition temperature. To speed up the simulations, the alignment of azos perpendicular to the polarization direction is enforced by the light-induced orientation potential that arises naturally from multiple cycles of photoisomerization.[19,28] The main questions we would like to answer are: (1) is it possible to observe the orientation or stretching of acrylate backbones along the polarization direction in fully atomistic simulations? (2) If so, what parameters would define the separation of time scales between the orientation of azos and the stretching of backbones? (3) Does the length of the main chains matter? We invite a fellow reader to follow us on this quest, which will hopefully provide valuable insights into the nature of polarized light-induced processes at the microscopic scale.

Fully atomistic model

Preparation of amorphous azo-polymer

The all-atom model of azo-monomer is built in Materials Studio 9.0.[32] The monomeric unit has acrylate backbone and a side-chain composed of 4-methoxyazobenzene grafted to a backbone at azobenzene's 4′-position *via* ethyloxy group, as depicted in Fig. 1b. The geometry of the monomeric unit is optimized for the *trans*-isomer of azo-group, using Forcite module with the following settings: polymer-consistent force field (PCFF),[33] Smart optimization algorithm (energy convergence 2×10^{-5} kcal mol^{-1}, force convergence tolerance 0.001 kcal mol^{-1} Å^{-1}, displacement convergence 10^{-5} Å).

This optimized geometry is further used for "polymerization" procedure in AMBER software.[34] The azo-polyacrylate used in the experiments[30,31] has an average chain length of 82 monomeric units (molecular weight M_w = 27 000). Performing atomistic simulations of multiple chains of this length at the experimental density is computationally infeasible, as even a single chain requires a cubic simulation box with a minimum edge length of L = 36 Å. To obtain a statistically representative ensemble and to assess possible chain-length effects, we therefore modeled two compositions: oligomers with chain lengths of N_{mol} = 10 and 20 monomeric units and with number of chains in the simulation box n = 96 and 48, respectively. Both oligomers are constructed in a head–tail configuration and exhibit atactic stereochemistry. The general AMBER force field (GAFF)[35] is applied for the parametrization of the bonded and non-bonded interactions in the simulated compositions. This force field has been validated for the simulations of various azo-containing materials.[36–38] The most important parameters for our simulation to take into account are (i) the parameters for the torsion angle of the azo-group preventing the *trans–cis* transition and keeping this mesogenic group planar and (ii) the dihedrals for the proper rotation of the side chains around the bond of the attachment to the main chain. The torsional barrier for the azo-group is set artificially high. The reason for this is that we are considering wavelengths of light, at which most

azo-chromophores are in the *trans*-state, and that the cycling between two isomers is reduced to the effective orientation potential, which will be introduced in the next section. The dihedrals define the strength of the "side-chain-backbone" coupling, *i.e.* the ability to transmit the torque acting on the azo-group to the main polymer chain, as given within the concept of the orientation approach.[13,28,39]

Initially, in the cubic periodic simulation boxes with $L = 150$ Å for $N_{mol} = 10$ and $L = 200$ Å for $N_{mol} = 20$, the stretched polymer chains are arranged in an array with their backbones oriented parallel to each other. Using first NVT molecular dynamics simulations implemented in LAMMPS,[40] the systems were equilibrated to an amorphous state[41] at $T = 1000$ K (Nosé–Hoover thermostat). Then we applied NPT molecular dynamics simulations at normal pressure $P = 1$ atm $\approx 10^{-4}$ GPa (Nosé–Hoover barostat) over a simulation time of 10 ns with a time step of 1 fs. Non-bonded van der Waals interactions are truncated at a cutoff distance of 12 Å, while long-range electrostatic interactions are computed using the particle–particle particle–mesh (PPPM) summation technique. Partial atomic charges are assigned based on the restrained electrostatic potential (RESP) fitting method.[42] The resulting density at $T = 1000$ K is about 0.76 g cm^{-3} for both compositions.

Glass transition temperature

Next, the glass transition temperature should be determined. From experiments of Ambrosio *et al.*[29] the glass transition temperature for the same azo-polyacrylate with $N_{mol} = 82$ monomeric units is $T_g = 67$ °C. Above this temperature the sample is in nematic state until it isotropizes at $T_{iso} = 113$ °C. The most common method for determining glass transition temperature in MD simulations involves monitoring the density of the polymer as a function of temperature.[24] Here, NPT simulations are performed over a range of temperatures, starting from a high-temperature equilibrium state (1000 K) down to cryogenic temperatures (100 K), with stepwise cooling (100 K step). At each temperature, the system is equilibrated for at least 10 ns. The transition from a fluid-like to a glassy state is identified by a change in the slope of the density-temperature curve, presented in Fig. 2. The glass transition temperature is observed to be approximately 450 K. The predicted T_g exhibits only marginal dependence on the molecular mass, consistent with recent findings from systematic all-atom simulations.[43] Interestingly, this all-atom T_g prediction is in excellent agreement with earlier coarse-grained simulations, which reported $T_g \approx 445$ K for the same polymer architecture.[24,44] This remarkable consistency across different levels of resolution confirms the robustness of the simulated T_g and highlights that both modeling approaches capture the essential role of azobenzene side-chains and backbone rigidity in the glass transition. The agreement between coarse-grained and all-atom models thus provides strong support for the transferability of simulation results and suggests that simplified models can reliably reproduce key thermophysical properties such as T_g.

It is worth noting that the simulated T_g of about 450 K significantly exceeds the experimental value of 340 K reported by Ambrosio *et al.*[29] Such a discrepancy is a well-known feature of fully atomistic simulations and may be attributed to several factors. First, the cooling rates accessible in MD simulations are orders of magnitude faster than those in experiment, leading to a systematic upward shift of T_g. Second, limitations in the force-field parametrization, particularly in describing subtle balances of non-bonded interactions and torsional potentials, can bias the absolute position of the transition. Taken together, these factors highlight that the simulated T_g should be interpreted in a relative rather than absolute sense, while still offering a reliable framework for understanding the underlying molecular mechanisms.

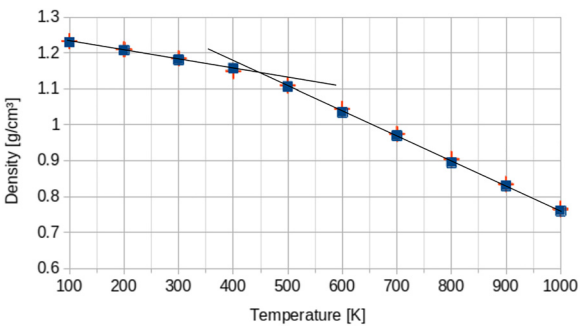

Fig. 2 Determination of the glass transition temperature $T_g \approx 450$ K from the change in density slope for two simulated chain lengths $N_{mol} = 10$ (blue squares) and 20 (red crosses).

Light-induced orientation potential

The kinetics of the photoisomerization process and light-induced ordering in azo-containing materials have been studied in detail in the ref. 28 and 45. Here, we briefly describe the key features that allow the introduction of an effective orientation potential, the use of which significantly reduces the computational effort. It is well known that the angle-selective absorption of photons by the *trans*-isomers causes an orientation of their long axes in a direction perpendicular to the light polarization $\boldsymbol{E}$. The stationary state is reached after tens of photo-isomerization cycles.[45] Although the absorption of photons by the *cis*-isomers is not angular-selective, their population becomes enriched around $\boldsymbol{E}$ due to the depletion of a number of *trans*-isomers in the same direction. The orientational states of *trans*- and *cis*-populations have been described by the two order parameters S_T and S_C in respect to $\boldsymbol{E}$ and their relative fractions Φ_T and $\Phi_C = 1 - \Phi_T$. The time evolution of these four parameters and their stationary values strongly depend on the ratio $\tilde{P}_C = P_C/P_T$ between the probabilities of *cis–trans* and *trans–cis* isomerization. The average order parameter $\bar{S} = \Phi_T S_T + \Phi_C S_C$ for all chromophores is shown to be nearly zero for short wavelengths ($\lambda \leq 400$ nm), when $\tilde{P}_C$ falls to 0.1 and $\Phi_C \geq 0.9$. Contrary, at longer wavelengths ($\lambda \geq 480$ nm), when $\tilde{P}_C$ increases to 10 and $\Phi_C \leq 0.1$, the average order parameter has large negative values. More importantly, its time evolution can be very well described with the help of effective orientation potential

$$U = V_0(\boldsymbol{u}\cdot\hat{\boldsymbol{E}})^2 = V_0\cos^2\theta, \quad (1)$$

where $\boldsymbol{u}$ is the unit vector of azobenzene orientation, $\hat{\boldsymbol{E}}$ is the unit vector of light polarization and θ is the angle between these two vectors. The strength of potential $V_0 \sim kTP_T/D$ is defined by the probability of *trans–cis* isomerization P_T and the orientation diffusion coefficient of the azobenzene D. The ratio kT/D is proportional to the material viscosity η which is known to increase exponentially with the decrease of absolute temperature T and reach the value of 10^3 GPa s at the glass transition temperature T_g. This implies that the strength of potential should increase upon cooling the material at the same illumination intensity.

The effective orientation potential (1) exerts a torque $\boldsymbol{M}$ in the azimuthal direction $\hat{\phi}$

$$\boldsymbol{M} = -\boldsymbol{u}\times\nabla_{\boldsymbol{u}}U = V_0\sin 2\theta\hat{\phi}, \quad (2)$$

that acts collectively on all atoms of the rigid azo-unit, causing them to rotate in concert. As can be seen from eqn (2), torque is measured in the same units as potential energy and has a maximum magnitude of V_0 when $\theta = 45^\circ$. In this study, we applied the light-induced torques with the values of V_0 ranging from 5 to 40 kcal mol^{-1}. These values correspond to 3.5–27.8 10^{-20} J and are one order of magnitude higher than those used in coarse-grained modeling of amorphous azo-polymers.[24] There, the sample density was about half as high, which probably explains lower values of the applied torques.

The magnitude of light-induced stress acting on azo-chromophores in the beginning of irradiation can be estimated as follows:[22,28]

$$\tau_0 = 2nV_0/5 \quad (3)$$

where n is the number density of chromophores. It slightly increases with the decrease of temperature due to a higher density of the simulated box. Let's choose $T = 550$ K, at which the box has the edges of about 80 Å. There are 960 azo-chromophores in the box. This gives $n = 1.875\times10^{27}$ m^{-3}, which is very close to the value of 1.5×10^{27} m^{-3} used in our previous theoretical studies.[28,39] For the light-induced torque $V_0 = 10$ kcal mol^{-1} $\approx 6.95\times10^{-20}$ J, the estimated stress magnitude is 130 MPa. Such a high stress is required to observe the reorientation of chromophores within a few tens of nanoseconds, which are accessible in fully atomistic MD simulations.

Light-induced effects at different temperatures and light intensities

The order and shape parameters

After equilibration at different temperatures and normal pressure, we switch on the orientation potential and analyze the real-time behavior of light-induced orientation and deformation in azo-polyacrylate samples. The orientational order parameter for azo-chromophores

$$S_{azo} = \left\langle \frac{3}{2}(\boldsymbol{u}\cdot\boldsymbol{n})^2 - \frac{1}{2}\right\rangle \quad (4)$$

is defined in respect to the spontaneous nematic director $\boldsymbol{n}$. It aligns along the polarization direction of light under the action of orientation potential. The angular brackets designate an averaging over all chromophores, orientation of which is characterized by the unit vectors $\boldsymbol{u}$. The orientation order of oligomer backbones is described by the order parameters S_i calculated in respect to the coordinate axes $\boldsymbol{i} = \boldsymbol{x}, \boldsymbol{y}$ and $\boldsymbol{z}$:

$$S_i = \left\langle \frac{3}{2}(\boldsymbol{b}\cdot\boldsymbol{i})^2 - \frac{1}{2}\right\rangle \quad (5)$$

The averaging is carried out over all oligomer backbones, whose orientation is characterized by the unit vectors $\boldsymbol{b}$. We also use the backbone sizes l_x, l_y, l_z, determined as the distances between maximum and minimum atom coordinates for the corresponding direction.

The directional photodeformations are monitored following dimensions of the volume element L_x, L_y, L_z, *i.e.*, the lengths of the periodic simulation box, which evolve self-consistently under constant-pressure conditions (NPT ensemble). Following our previous publication,[44] the orientation distribution of azo-chromophores around the oligomer backbones is characterized by the polar angle $\alpha = \arccos|\boldsymbol{u}\cdot\boldsymbol{g}_{max}|$. It is measured between the orientation vector $\boldsymbol{u}$ of the chromophore and the main eigenvector $\boldsymbol{g}_{max}$ of the gyration tensor of the backbone. Only the smallest angle is chosen, since the orientation states with α and $180^\circ - \alpha$ should be equiprobable for side-chain azo-polymers with the head–tail symmetry.[39]

Reorientation of azobenzene chromophores

We begin by analyzing the orientational order parameter of chromophores S_{azo}. In the absence of light, S_{azo} fluctuates around zero, which is a typical behavior for isotropic systems of nanoscopic size.[24] After the light is switched on, the azo-chromophores reorient perpendicular to the light polarization $\boldsymbol{E}$, that breaks the symmetry of initially isotropic system. The spontaneous nematic director in eqn (4) aligns along the polarization direction, $\boldsymbol{n} = \hat{\boldsymbol{E}}$. Note that such a nematic state is characterized by negative values of the order parameter $-0.5 \le S_{azo} < 0$. Therefore, S_{azo} decreases monotonically with time under light irradiation and finally reaches the steady state plateau, whose value depends on the light intensity and temperature. At $T = 550$ K, the plateau value for light-induced torques $V_0 \ge 5$ kcal mol^{-1} is below -0.4, indicating a strong reorientation into the plane perpendicular to $\boldsymbol{E}$ (Fig. 3a).

Our simulations clearly show several timescales. For $T > T_g$, one can distinguish at least three different regimes of time evolution in the double logarithmic representation. As an example, we show in Fig. 3b the simulations results at $T = 550$ K. The first time t_1 characterizes the delayed reaction of single azo-chromophores on the orientation potential. It decreases with the increase of light-induced torque: t_1 is about 0.01 ns for $V_0 = 5$ kcal mol^{-1} and 0.001 ns for $V_0 = 15$ kcal mol^{-1}. At $t_1 < t < t_2$, the azo-chromophores reorient collectively which is reflected by exponential growth of the order parameter magnitude $|S_{azo}|$. Finally, at $t > t_2$, the order parameter slowly approaches the steady state value. Since the time t_2 also decreases with the increase of V_0, the regime of exponential

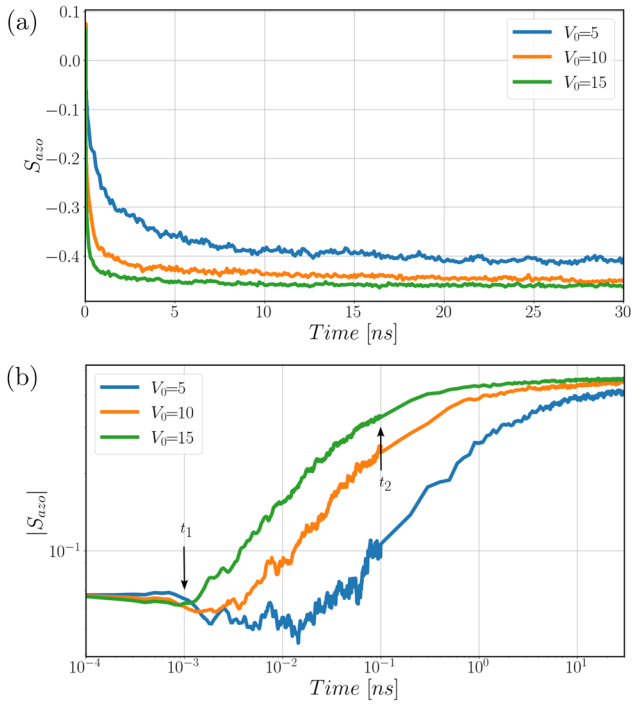

Fig. 3 (a) Orientational order parameter S_{azo} for N_{mol} = 20 at T = 550 K and different light-induced torques V_0 in kcal mol^{-1}. (b) The double-logarithmic plot shows that time evolution of the order parameter magnitude $|S_{azo}|$ exhibits three regimes: (1) initial delay in reorientation, (2) exponential growth, (3) slow approach to the steady state.

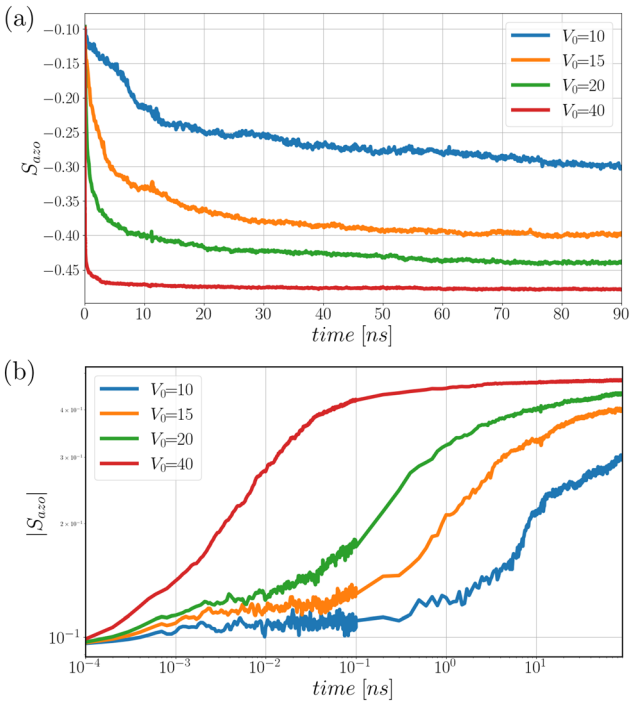

Fig. 4 (a) Orientational order parameter S_{azo} for N_{mol} = 20 at T = 400 and different light-induced torques V_0. (b) The double-logarithmic plot shows that time evolution of the order parameter magnitude $|S_{azo}|$ exhibits three regimes: (1) slow exponential growth, (2) fast exponential growth, (3) slow approach to the steady state.

growth stretches approximately over the same two decades for all values of V_0.

The similar behavior for time evolution of S_{azo} is observed at $T < T_g$ but at larger values of the light-induced torque V_0. As an example, we show the simulations results at T = 400 K in Fig. 4. To achieve the same degree of reorientation, for instance S_{azo} = −0.4, it is necessary to apply V_0 = 15 kcal mol^{-1}, three times larger torque than at T = 550 K (compare with Fig. 3). Interestingly, at low temperatures, there is no initial delay in the orientation process: the order parameter magnitude begins to increase immediately after application of the light-induced torque. However, the reorientation takes much longer time, which is clearly evident at V_0 = 10 kcal mol^{-1}, where the steady state is not yet reached after 90 ns.

It is instructive to compare the reorientation of azo-chromophores at the same V_0 but different temperatures (Fig. 5). Reorientation occurs very rapidly (∼10 ns) at all three temperatures above T_g and starts to slow down at T_g. Nevertheless, the order parameter appears to approach the same steady-state value of −0.45.

Directional photodeformations

Linearly polarized light causes uniaxial stretching of azo-polymer microposts[16,19] and colloids[18,22] along the polarization direction, while preserving their volume. The same effect can be investigated in fully atomistic MD simulations by tracking the temporal evolution of the dimensions of a nanoscopic sample. Irradiation

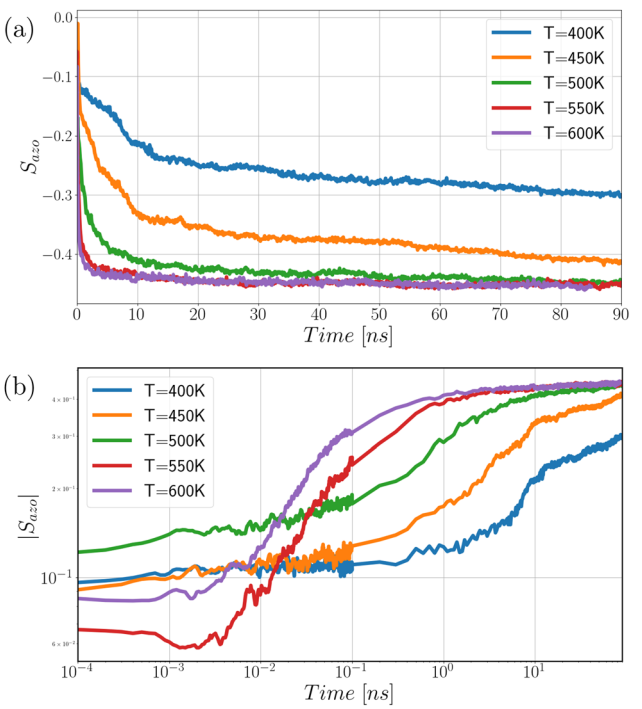

Fig. 5 (a) Orientational order parameter S_{azo} for N_{mol} = 20 at V_0 = 10 kcal mol^{-1} and different temperatures T. (b) The double-logarithmic plot shows that time evolution of the order parameter magnitude $|S_{azo}|$.

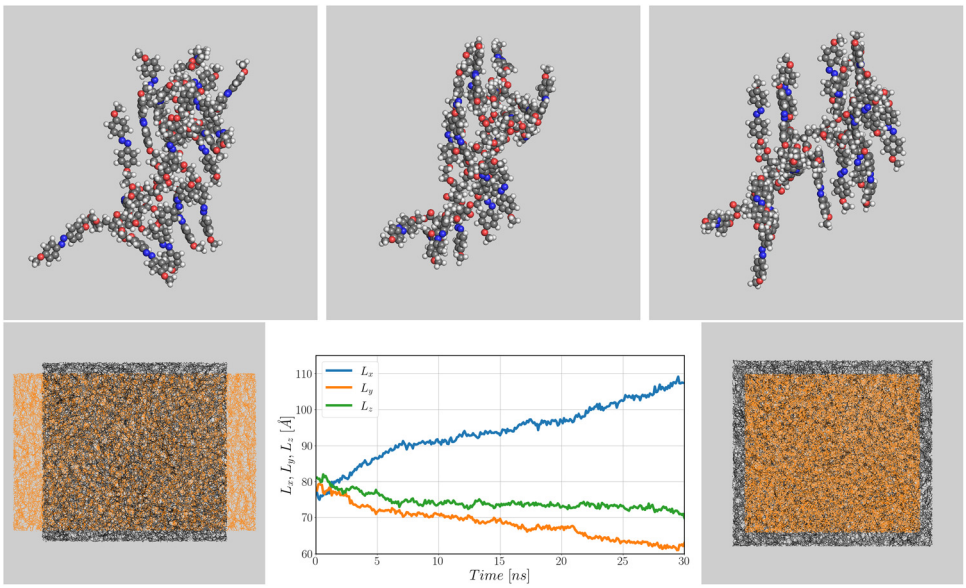

Fig. 6 (Top) The snapshots of an acrylate oligomer with 20 azo-chromophores: before irradiation, after 1 ns and 30 ns of irradiation. (Bottom) The dimensions of volume element: L_x along $\boldsymbol{E}$ and L_y, L_z perpendicular to $\boldsymbol{E}$ (center). The superimposed snapshots of simulation box before and after 30 ns irradiation: *xz*-projection on the left and *yz*-projection on the right. T = 550 K and V_0 = 15 kcal mol^{-1}.

of the samples with the light linearly polarized along the *x*-, *y*- and *z*-axes showed no differences at any temperature. This further confirms the isotropic orientation of the azos and polymer backbones in as-prepared samples. In the following we present the results of irradiation with light polarized along the *x*-direction.

Consider first the temperatures above the glass transition, for example T = 550 K (central plot in Fig. 6). The dimension of volume element L_x along the light polarization $\boldsymbol{E}$ first decreases from 80 Å (the equilibrium value) to 75 Å, after which it continuously grows, reaching 110 Å after 30 ns of the irradiation. The dimensions L_y and L_z perpendicular to $\boldsymbol{E}$ decrease. The snapshots of the simulation box before and under irradiation confirm a uniaxial type of light-induced deformation. A slight contraction of the box in the polarization direction occurs between times t_1 and $t_2 \sim 1$ ns, when the order parameter of azobenzenes S_{azo} decreases exponentially. Comparing the snapshots of an azo-oligomer at equilibrium and after 1 ns of irradiation (Fig. 6 top), a noticeable compactization of the molecule along $\boldsymbol{E}$ is noted. This compactization happens due to alignment of azobenzenes in the plane perpendicular to $\boldsymbol{E}$. The polymer backbone appears to keep its shape until the same moment t_2. However, after that, when the orientation state of azo-chromophores does not change much, the polymer backbone begins to align and slightly stretch along $\boldsymbol{E}$. Such behavior has been predicted by analytical theory[39] and also found in coarse-grained simulations.[25] Notably, we did not observe any helicity in the molecular conformations, either at equilibrium or under irradiation.

Interestingly, the light-induced torques $5 \leq V_0 \leq 15$ kcal mol^{-1} cause comparable elongation of the volume element after 30 ns of irradiation at T = 550 K, only the duration of initial contraction regime decreases with the increase of V_0 (Fig. 7a). However, at low temperatures $T < T_g$, only contraction of the volume element along $\boldsymbol{E}$ is observed (Fig. 7b). L_x decreases considerably with the increase of light-induced torque V_0. This happens at the beginning of irradiation, when the order parameter magnitude of azobenzenes grows exponentially with time (Fig. 4). At larger times, there is no change in the dimensions of the simulation box. The stretching of volume element is not observed, because the conformations of polymer backbones stay frozen at $T < T_g$, as we discuss in the next section.

Alignment of polymer backbones

Let us analyze the origin of the long-time stretching of the volume element at elevated temperatures $T > T_g$. The orientation of oligomer backbones with respect to the light polarization is described by the order parameter S_x, as defined in eqn (5).

Its magnitude increases from the equilibrium value 0 to about 0.25 for T = 550 K and a light-induced torque V_0 = 10 kcal mol^{-1} (Fig. 8a). As expected, the order parameters S_y and S_z take negative values, since the sum of S_i should be zero. Although both S_y and S_z fluctuate noticeably, they reach a similar steady-state value of -0.12 ± 0.02, indicating a uniaxial orientational order. The average sizes of the oligomer backbones also show large fluctuations, but the trend is clear. The backbones align along the polarization direction x, resulting in an increase in l_x and a decrease in l_y and l_z (Fig. 8b). Above the glass transition, the conformations of the polymer backbones are not frozen and can change under irradiation. However, the average length of the oligomer backbones, calculated as $l = \sqrt{l_x^2 + l_y^2 + l_z^2}$, fluctuates around 60 Å without any stretching or contraction (Fig. 8c). From this we can conclude that the origin of directional photodeformations above the glass transition is the alignment of backbones along the light polarization.

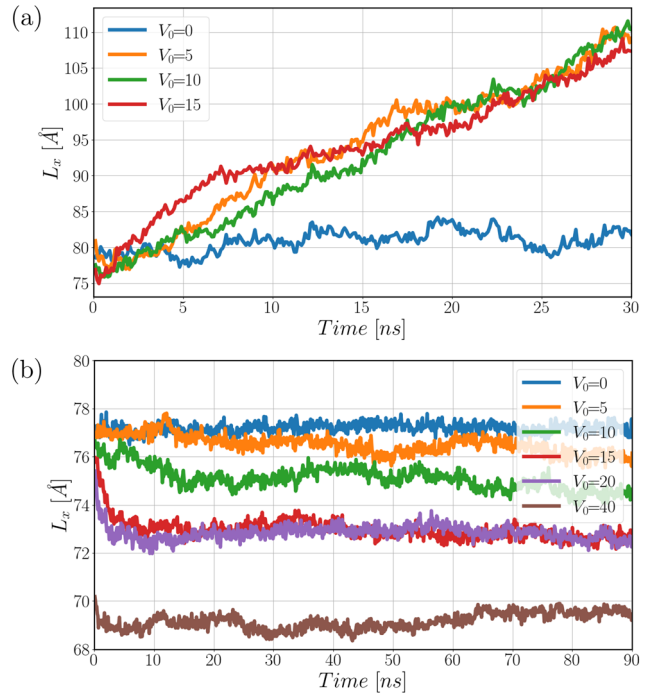

Fig. 7 The dimension of volume element L_x along the polarization direction $\boldsymbol{E}$ for N_{mol} = 20 and different light-induced torques V_0. (a) Slight contraction followed by stretching at T = 550 K, (b) contraction at T = 400 K.

In the glassy state, at $T < T_g$, we found no evidence of alignment or deformation of the oligomer backbones even after 90 ns of simulation time. Both the order parameters (Fig. 9a) and the average sizes (Fig. 9b) fluctuate around their equilibrium values. The average length of the oligomer backbones fluctuates around 60 Å (Fig. 9c), the same value as at T = 550 K. The fast oscillations of l_x observed in the glassy state can be attributed to an elastic transient response of the oligomer backbones induced by rapid reorientation of the azo chromophores. Above the glass transition temperature, the increased molecular mobility makes the response predominantly dissipative, and the oscillations are therefore strongly damped.

To elucidate the differences in behavior below and above the glass transition, we examined how a light-induced torque influences the orientation distribution of azo-chromophores around the oligomer backbones. This distribution is defined by the polar angle α, which is measured as described above. The corresponding histograms are presented in Fig. 10. They can be characterized by the average polar angle $\langle\alpha\rangle$ and the shape factor

$$q = \left\langle \frac{3}{2}\cos^2\alpha - \frac{1}{2} \right\rangle. \quad (6)$$

Above the glass transition at T = 550 K, $\langle\alpha\rangle$ is approximately 53° in the dark and decreases only slightly by 2° when a light-induced torque of V_0 = 10 kcal mol^{-1} is applied for 30 ns. The shape factor q increases from 0.10 to 0.13 over the same period. A closer look shows that the histogram widens after 30 ns irradiation (Fig. 10a), and forms a kind of two maxima at 35° and 65°.

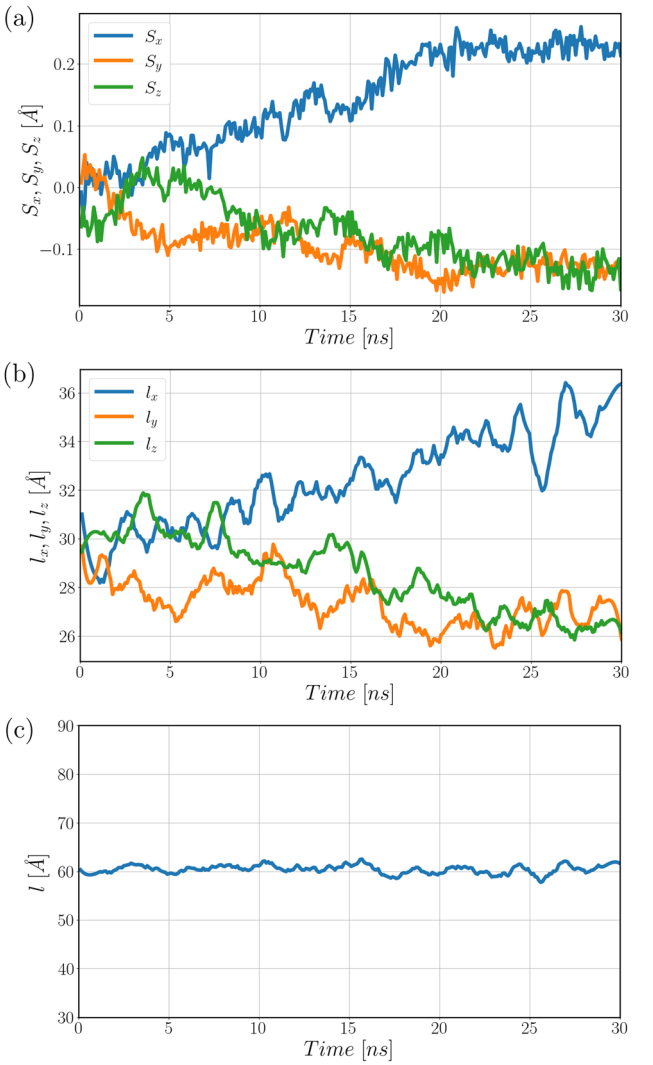

Fig. 8 (a) Orientational order parameters S_x, S_y, S_z of oligomer backbones, (b) average backbone sizes l_x, l_y, l_z and (c) their average length l for N_{mol} = 20 at T = 550 K and V_0 = 10 kcal mol^{-1}.

A similar trend is observed below the glass transition at T = 400 K for the same torque value. At a higher torque of V_0 = 40 kcal mol^{-1}, the peak of the histogram shifts to smaller values of the polar angle (Fig. 10b). The average polar angle $\langle\alpha\rangle$ decreases from 53° to 48° within the first nanosecond of irradiation, and the shape factor increases from 0.08 to 0.20. Extending the irradiation to 90 ns leads to only marginal additional changes in both quantities.

Previous theoretical studies[39,44] correlated positive values of the shape factor with contraction of an azo-polymer, when the side chains are rigidly coupled to the main chain. In contrast, we observe above the glass transition an elongation of the azo-polyacrylate, which is characterized by $q \sim 0.1$ in fully atomistic MD simulations. This discrepancy suggests that the flexible spacer plays a crucial role in mediating the transfer of light-induced torque from the azo-chromophores to the oligomer backbones. We investigate this effect in more detail in the following subsection.

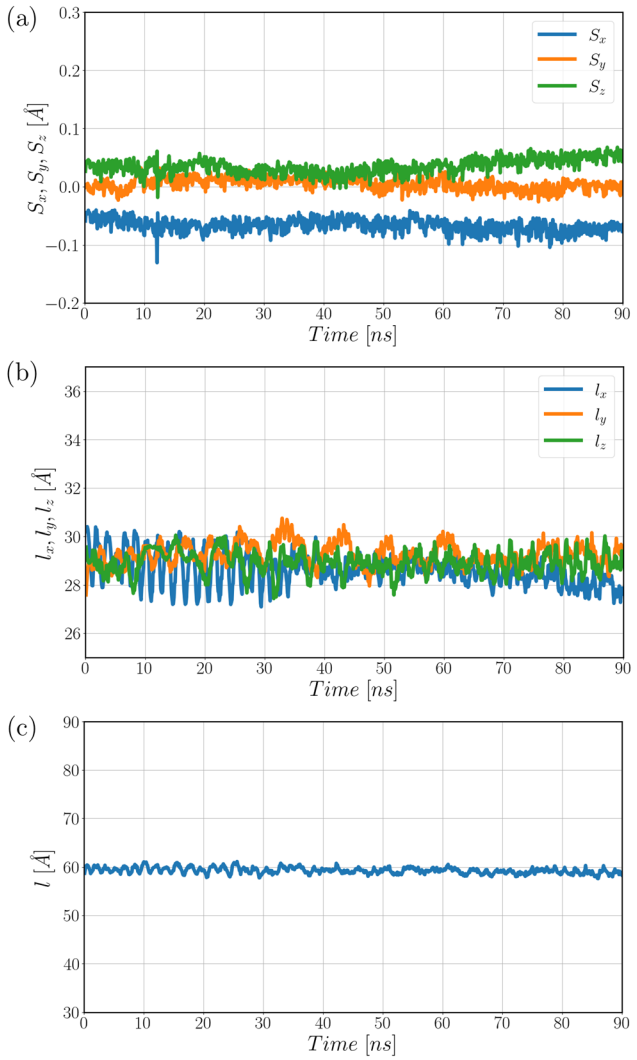

Fig. 9 (a) Orientational order parameters S_x, S_y, S_z of oligomer backbones, (b) average backbone sizes l_x, l_y, l_z and (c) their average length l for N_{mol} = 20 at T = 400 K and V_0 = 10 kcal mol^{-1}.

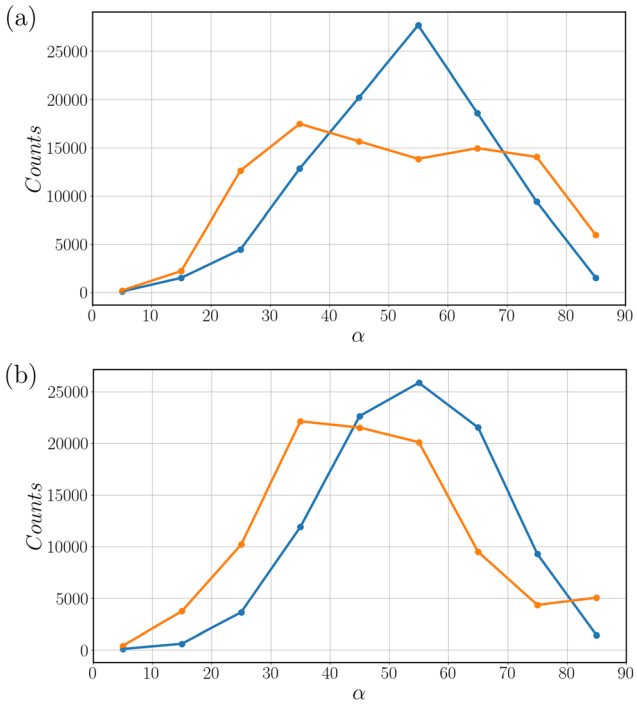

Fig. 10 Histogram of polar angle α at (a) T = 550 K and (b) T = 400 K. The blue curves are produced in the dark (V_0 = 0) and the orange curves under light irradiation: (a) V_0 = 10 kcal mol^{-1} and (b) V_0 = 40 kcal mol^{-1}.

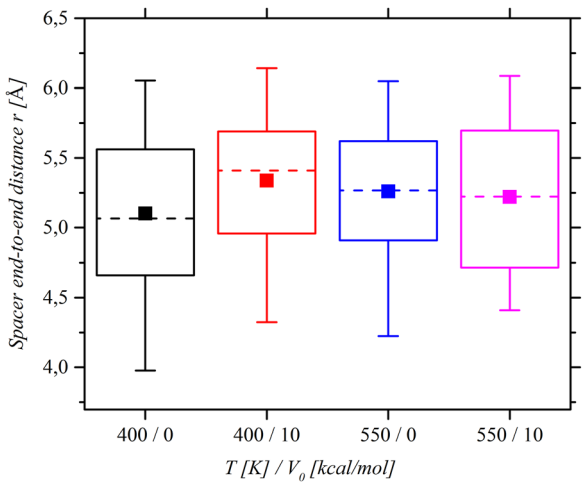

Fig. 11 End-to-end distance r of the spacer for N_{mol} = 20 below (T = 400 K) and above (T = 550 K) the glass transition temperature in the dark (V_0 = 0) and under light irradiation (V_0 = 10 kcal mol^{-1}). The boxes represent the inter-quartile range (25–75%). Filled squares denote the mean spacer r length for each system. Whiskers extend to 1.5 times the inter-quartile range.

The role of spacer in torque transfer

The chemical linkage between the azo-chromophore and the polymer backbone (Fig. 1b) contains a flexible alkyloxy–ester spacer that provides several torsional degrees of freedom. Above the glass transition temperature, internal rotations around C–O and C–C bonds are frequently observed in fully atomistic MD simulations. This leads to a broad distribution of spacer conformations, including both extended (all-*trans*) and folded geometries due to *gauche*- and, in some cases, *cis*-like arrangements. As expected, cooling below the glass transition suppresses internal rotations, and the spacer conformations remain frozen in MD simulations.

The light-induced orientation of azo-chromophores may cause additional conformational changes, the most likely being mechanical stretching of the spacer. To verify this, we analyzed the length (end-to-end distance) r of the spacer in the dark and under light irradiation for two temperatures, below and above the glass transition. At T = 550 K, the mean spacer length (filled squares in Fig. 11) is 5.25 Å in the dark and does not change under light irradiation. However, the inter-quartile range of the r-distribution broadens, indicating an enrichment of more extended and more folded conformations. This observation correlates with the broadening of the histogram for the polar angles α under the same conditions (Fig. 10a). Lowering the

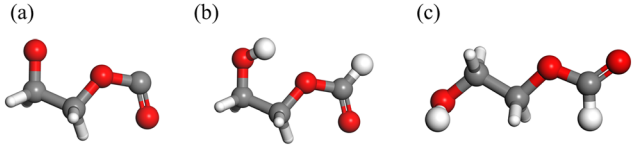

Fig. 12 (a) Spacer fragments are extracted from equilibrated MD trajectories of the polymer matrix. Here, one example is shown "as-cut". (b) The truncated fragment is chemically capped by adding two hydrogen atoms to restore closed-shell valency. (c) Local minimum-energy conformation of isolated 2-hydroxyethyl formate after optimization.

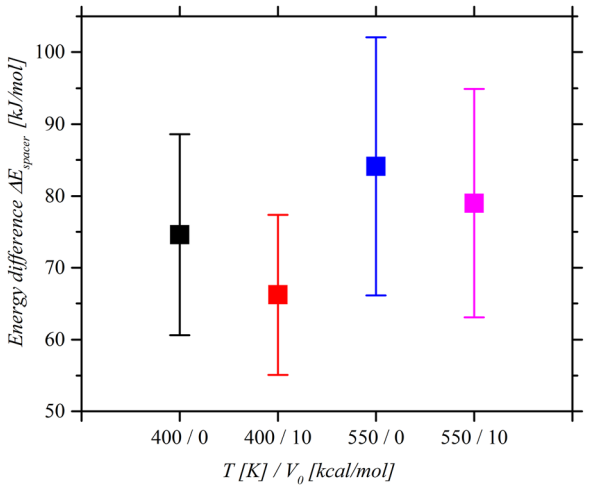

Fig. 13 Energy difference ΔE_{spacer} for spacer units in a fixed geometry, evaluated at temperatures T = 400 and 550 K in the dark (V_0 = 0) and under light irradiation (V_0 = 10 kcal mol^{-1}). The reference energy corresponds to the optimized ground-state geometry of isolated 2-hydroxyethyl formate. Single-point energy calculations were performed for spacer fragments extracted from five randomly selected polymer chains with N_{mol} = 20, resulting in a total of 100 DFT calculations for each data point shown.

temperature to T = 400 K below the glass transition causes a slight decrease in the mean spacer length to 5.1 Å. Interestingly, applying a light-induced torque leads to an increase in the average spacer length to 5.3 Å and a decrease in the interquartile range, which suggests a shift towards more extended conformations, compared to the dark state. This would explain the light-induced reduction of the average polar angle $\langle\alpha\rangle$ in Fig. 10b. In all cases, the mean spacer length stays well below the fully extended all-*trans* limit (*ca.* 6 Å). These results indicate that the transfer of light-induced torque from the azochromophores to the backbones is not accompanied by significant geometric stretching of the spacer. The presence of several rotatable bonds allows the spacer to accommodate the torque transfer through torsional adjustments above the glass transition and slight stretching below the glass transition.

Fig. 12 illustrates workflow used to generate the reference ground-state structure of 2-hydroxyethyl formate for the spacer energetics analysis. Panel (a) displays a spacer fragment directly extracted from an oligomer chain as sampled in the MD trajectory. This "as-cut" fragment reflects the instantaneous, thermally accessible conformation of the spacer, including torsional distortions and deviations from an idealized all-*trans* geometry. In panel (b), the same fragment is shown after saturation with two hydrogen atoms, which restores chemical valency and produces a closed-shell molecule suitable for density functional theory (DFT) calculations. This H-saturated structure is used as the starting geometry for further DFT calculations. Note that the original atoms keep their coordinates/positions as on Panel (a). Panel (c) shows the fully DFT optimized ground-state geometry of the resulting molecule of 2-hydroxyethyl formate. This structure represents the local minimum-energy reference state against which the energetic cost of thermally and torque-induced spacer distortions is evaluated. To quantify the conformational flexibility of the spacer, we compared the energy of the fully optimized ground-state geometry of 2-hydroxyethyl formate molecule with the computed energies of spacer conformations extracted from the MD trajectory. The comparison was done for a system of longer chains containing N_{mol} = 20 units (Fig. 13). All DFT calculations are performed in Gaussian 09 Rev. E01 software[46] with Perdew–Burke–Ernzerhof (PBE) functional and 6-31G* basis set. Note that we additionally calculated the energy differences for the same set of spacers using the hybrid B3LYP functional with 6-31G* basis set. Although a direct comparison of energies obtained with different density functionals is not strictly meaningful, both methods exhibit the same qualitative trend, supporting the robustness of the observed temperature-dependent behavior.

First, for all simulated conditions, the ΔE_{spacer} is strictly positive, on the order of *ca.* 65–85 kJ mol^{-1}, indicating that spacer conformations sampled within the polymer matrix correspond to energetically less favourable states relative to the optimized ground-state geometry of isolated 2-hydroxyethyl formate. This reflects the fact that spacers in the condensed polymer environment simultaneously populate multiple non-optimal torsional states and experience geometric distortions imposed by chain packing and connectivity.

Second, temperature has a pronounced effect on both the mean value and the spread of ΔE_{spacer}. At T = 550 K, the average energy difference is systematically higher and the distribution broader than at T = 400 K. This trend is consistent with enhanced conformational sampling at elevated temperatures, where thermal fluctuations allow the spacer to explore a wider range of torsional conformations, including higher-energy *gauche* and partially folded states. In contrast, 50 K below the glass transition at T = 400 K, the distribution of ΔE_{spacer} is narrower, reflecting reduced conformational freedom and partial freezing of spacer dynamics.

Third, the influence of the light irradiation is comparatively weak. The mean values of ΔE_{spacer} decrease under application of the light-induced torque (V_0 = 10 kcal mol^{-1}) by 6 kJ mol^{-1} at T = 550 K and slightly more by 8 kJ mol^{-1} at T = 400 K. The latter observation correlates with a shift towards more extended spacer conformations, as shown in Fig. 11. Nevertheless, the changes are minor, and there is no evidence of any significant stretching of the spacer towards an energetically favourable all-*trans* conformation under light irradiation.

Taken together, these trends demonstrate that the energetic state of the spacer is governed primarily by thermal effects rather than by the applied light irradiation. The spacer accommodates light-induced reorientation of azo-chromophores predominantly through internal torsional rearrangements, accompanied by a slight stretching below the glass transition. This conclusion is fully consistent with the earlier analysis of the spacer end-to-end distance and supports the picture of a flexible spacer that weakens direct torque transfer from the azo-chromophores to an acrylate backbone.

Conclusions

Fully atomistic MD simulations of dense azo-polyacrylate samples allow us now to answer the questions posed in the introduction to this study:

1. It is possible to observe the orientation of acrylate backbones along the polarization direction above the glass transition temperature. The simulation box first slightly contracts and then elongates in this direction.

2. The contraction of the box correlates with the rapid orientation of azobenzenes, followed by much slower orientation of main chains. The separation between these two time scales increases dramatically when the governing parameter temperature drops below the glass transition.

3. Doubling the length of the main chains does not affect the glass transition temperature or the light-induced processes in the simulated oligomers. This is due to the absence of entanglements in these short but densely grafted azo-polymer structures.

On the one hand, we obtained a very positive result, that fully atomistic MD simulations allow us to observe the orientation of acrylate backbones along the polarization direction, as predicted by analytical theories. On the other hand, our studies become hampered by extremely short observation times. This is an intrinsic limitation of all-atom MD simulations. Another valuable result is a better understanding of the nature of coupling between the orientation of photosensitive azobenzene groups and the backbones in a flexible polymer.

Indeed, in contrast to rigid azo-polyesters, the azo-polyacrylate examined here contains an alkyloxy–ester spacer that possesses several accessible torsional degrees of freedom. The MD trajectories reveal broad polar angle distributions and frequent sampling of *gauche* and partially folded states relative to an all-*trans* reference. This conformational richness allows the spacer to absorb a substantial part of the light-induced torque through torsional adjustments. As a result, the effective coupling between the chromophore and the backbone is significantly weaker than in architectures with short and rigid linkers. The torque imparted by photoaligned azobenzenes is therefore only partially transferred to the main chain and with a considerable delay. Increasing the temperature above the glass transition permits the backbones to respond during nanoscopic observation times.

This mechanistic picture explains why highly flexible azo-polyacrylates still display robust photodeformations in experiments.[14,29] While the side-chain/backbone coupling is attenuated, it is not eliminated, and its effect can be observed at ambient temperatures for hundreds of seconds. One aspect of superficial restructuring that often puzzles experimentalists is that it occurs much later than the formation of the preceding birefringence grating. Such a behavior cannot be explained by earlier models and is consistent only with the modern orientation approach.[13] As hypothesized in our previous studies,[12,25] this temporal delay can be attributed to the weak (non-rigid) coupling between the azobenzene side-chains and the polymer backbone, as well as to the much slower orientational process of the polymer backbones compared to the azo-chromophores. This hypothesis receives strong support from the present fully atomistic simulations. Another notable aspect is that irradiation with linearly polarized light does not introduce any helicity into the conformations of azo-acrylate chains. This result is important for understanding the action of structured light on azo-polyacrylate samples. If spiral surface patterns are observed upon irradiation,[29] their origin should therefore be sought not in the molecular architecture but in the polarization pattern of the light field.

Author contributions

The manuscript was written through contributions of all authors, and all authors have given approval to the final version. M. S. conceived the project and acquired funding. D. A. R. and O. G. carried out calculations and performed theoretical and computational analyses. Data curation and formal analysis were conducted by D. A. R., O. G., and M. S. Visualization was prepared by D. A. R. and O. G. M. S. supervised the project and coordinated research activities. The original draft was prepared by D. A. R., O. G., and M. S., and all authors contributed to reviewing and editing the manuscript.

Conflicts of interest

There are no conflicts of interest to declare.

Data availability

Data for this article, including ASCII files and *.xyz files containing the coordinates of the polymeric chains simulated at T = 400 K and 550 K, are available at Zenodo at https://doi.org/10.5281/zenodo.19091272.

Acknowledgements

Financial support from Deutsche Forschungsgemeinschaft (DFG) under grant GR 3725/10-1 is greatly appreciated. The authors gratefully acknowledge the computing time made available to them on the high-performance computer at the NHR Center of TU Dresden. This center is jointly supported by the Federal Ministry of Research, Technology and Space of Germany and the state governments participating in the NHR

(https://www.nhr-verein.de/unsere-partner). The authors acknowledge the valuable contribution of Dr Markus Koch, who developed and integrated an effective orientation potential[28,45] into the simulation code LAMMPS (https://github.com/Markus91Koch/LAMMPS_Extensions) as part of his PhD research, forming the methodological basis for the present study.

References

1 N. S. Yadavalli and S. Santer, *J. Appl. Phys.*, 2013, **113**, 224304.
2 N. S. Yadavalli, F. Linde, A. Kopyshev and S. Santer, *ACS Appl. Mater. Interfaces*, 2013, **5**, 7743–7747.
3 J. Jelken and S. Santer, *RSC Adv.*, 2019, **9**, 20295–20305.
4 P. Pagliusi, B. Audia and C. Provenzano, *et al.*, *ACS Appl. Mater. Interfaces*, 2019, **11**, 34471–34477.
5 H. Rekola, A. Berdin and C. Fedele, *et al.*, *Sci. Rep.*, 2020, **10**, 19642.
6 Y. Lim, B. Kang, S. J. Hong, H. Son, E. Im, J. Bang and S. Lee, *Adv. Funct. Mater.*, 2021, **31**, 2104105.
7 S. L. Oscurato, F. Reda, M. Salvatore, F. Borbone, P. Maddalena and A. Ambrosio, *Laser Photonics Rev.*, 2022, **16**, 2100514.
8 J. Strobelt, M. Van Soelen, H. Abourahma and D. J. J. McGee, *Adv. Opt. Mater.*, 2023, **11**, 2202245.
9 L. Marrucci, C. Manzo and D. Paparo, *Phys. Rev. Lett.*, 2006, **96**, 163905.
10 A. Forbes, M. de Oliveira and M. Dennis, *Nat. Photonics*, 2021, **15**, 253–262.
11 L. Nikolova, L. Nedelchev, T. Todorov, T. Petrova, N. Tomova, V. Dragostinova, P. Ramanujam and S. Hvilsted, *Appl. Phys. Lett.*, 2000, **77**, 657–659.
12 N. Tverdokhleb, B. Audia, P. Pagliusi and M. Saphiannikova, *J. Mater. Chem. C*, 2025, **13**, 1263–1271.
13 M. Saphiannikova, V. Toshchevikov and N. Tverdokhleb, *Soft Matter*, 2024, **20**, 2688–2710.
14 I. K. Januariyasa, F. Reda, N. Liubimtsev, P. Patel, C. Pedersen, F. Borbone, M. Salvatore, M. Saphiannikova, D. J. McGee and S. L. Oscurato, Accepted at Light: Science & Applications https://arxiv.org/abs/2506.06857.
15 D. Bublitz, M. Helgert, B. Fleck, L. Wenke, S. Hvilsted and P. Ramanujam, *Appl. Phys. B: Lasers Opt.*, 2000, **70**, 863–865.
16 H. S. Kang, H.-T. Kim, J.-K. Park and S. Lee, *Adv. Funct. Mater.*, 2014, **24**, 7273–7283.
17 N. S. Yadavalli, T. Koenig and S. Santer, *J. Soc. Inf. Disp.*, 2015, **23**, 154–162.
18 S. Loebner, N. Lomadze, A. Kopyshev, M. Koch, O. Guskova, M. Saphiannikova and S. Santer, *J. Phys. Chem. B*, 2018, **122**, 2001–2009.
19 B. Yadav, J. Domurath, K. Kim, S. Lee and M. Saphiannikova, *J. Phys. Chem. B*, 2019, **123**, 3337–3347.
20 V. Toshchevikov and M. Saphiannikova, *Processes*, 2023, **11**, 129.
21 N. Tverdokhleb, S. Loebner, B. Yadav, S. Santer and M. Saphiannikova, *Polymers*, 2023, **15**, 463.
22 S. Loebner, B. Yadav, N. Lomadze, N. Tverdokhleb, H. Donner, M. Saphiannikova and S. Santer, *Macromol. Mater. Eng.*, 2022, **307**, 2100990.
23 W.-C. Xu, S. Sun and S. Wu, *Angew. Chem., Int. Ed.*, 2019, **58**, 9712–9740.
24 J. M. Ilnytskyi, D. Neher and M. Saphiannikova, *J. Chem. Phys.*, 2011, **135**, 044901.
25 J. M. Ilnytskyi, V. Toshchevikov and M. Saphiannikova, *Soft Matter*, 2019, **15**, 9894–9908.
26 M. Böckmann and N. Doltsinis, *J. Chem. Phys.*, 2016, **145**, 154701.
27 M. Merkel, A. Elizabeth, M. Böckmann, H. Mönig, C. Denz and N. L. Doltsinis, *J. Chem. Phys.*, 2023, **158**, 104905.
28 V. Toshchevikov, J. Ilnytskyi and M. Saphiannikova, *J. Phys. Chem. Lett.*, 2017, **8**, 1094–1098.
29 A. Ambrosio, L. Marrucci, F. Borbone, A. Roviello and P. Maddalena, *Nat. Commun.*, 2012, **3**, 989.
30 S. L. Oscurato, M. Salvatore, F. Borbone, P. Maddalena and A. Ambrosio, *Sci. Rep.*, 2019, **9**, 6775.
31 F. Reda, M. Salvatore, M. Astarita, F. Borbone and S. L. Oscurato, *Adv. Opt. Mater.*, 2023, **11**, 2300823.
32 BIOVIA, *Dassault Systemes, Materials Studio 9.0*, https://www.3ds.com/de/products/biovia/materials-studio.
33 H. Sun, S. J. Mumby, J. R. Maple and A. Hagler, *J. Am. Chem. Soc.*, 1994, **116**, 2978–2987.
34 D. Case, H. Aktulga, K. Belfon, D. Cerutti, G. Cisneros, V. Cruzeiro, N. Forouzesh, T. Giese, A. Götz and H. Gohlke, *et al.*, *J. Chem. Inf. Model.*, 2023, **63**, 6183–6191.
35 J. Wang, R. Wolf, J. Caldwell, P. Kollman and D. Case, *J. Comput. Chem.*, 2004, **25**, 1157–1174.
36 K. Moghaddam, G. Giudetti, W. Sipma and S. Faraji, *Phys. Chem. Chem. Phys.*, 2020, **22**, 26944–26954.
37 J. Ehrman, V. Lim, C. Bannan, N. Thi, D. Kyu and D. Mobley, *J. Comput.-Aided Mater. Des.*, 2021, **35**, 271–284.
38 H. Heinz, R. Vaia, H. Koerner and B. Farmer, *Chem. Mater.*, 2008, **20**, 6444–6456.
39 V. Toshchevikov, M. Saphiannikova and G. Heinrich, *J. Phys. Chem. B*, 2009, **113**, 5032–5045.
40 A. Thompson, H. Aktulga, R. Berger, D. S. Bolintineanu, W. M. Brown, P. S. Crozier, P. J. In't Veld, A. Kohlmeyer, S. G. Moore and T. D. Nguyen, *et al.*, *Comput. Phys. Commun.*, 2022, **271**, 108171.
41 D. M. Anstine, A. Strachan and C. M. Colina, *Modell. Simul. Mater. Sci. Eng.*, 2020, **28**, 025006.
42 C. I. Bayly, P. Cieplak, W. Cornell and P. A. Kollman, *J. Phys. Chem.*, 1993, **97**, 10269–10280.
43 M. Klajmon, V. Aulich, J. Ludik and C. Cervinka, *Ind. Eng. Chem. Res.*, 2023, **62**, 21437–21448.
44 M. Saphiannikova, V. Toshchevikov and J. Ilnytskyi, Nanoscopic actuators in light-induced deformation of glassy azopolymers, *Proceedings of Society of Photo-Optical Instrumentation Engineers (SPIE)*, 2013, pp. 243–250.
45 V. Toshchevikov, T. Petrova and M. Saphiannikova, *Soft Matter*, 2017, **13**, 2823–2835.
46 M. J. Frisch, G. W. Trucks, H. B. Schlegel, *et al.*, *Gaussian 09 Revision E.01*, Gaussian Inc., Wallingford CT, 2016.